JACS
JOURNAL OF THE AMERICAN CHEMICAL SOCIETY

Communication

Covalent Catalysis by Cross # Amyloid Nanotubes

Baishakhi Sarkhel, Ayan Chatterjee, and Dibyendu Das

J. Am. Chem. Soc., **Just Accepted Manuscript** • DOI: 10.1021/jacs.9b13517 • Publication Date (Web): 21 Feb 2020

Covalent Catalysis by Cross β Amyloid Nanotubes

Baishakhi Sarkhel, Ayan Chatterjee and Dibyendu Das*

Department of Chemical Sciences, Indian Institute of Science Education and Research (IISER) Kolkata, Mohanpur 741246, India

Supporting Information Placeholder

ABSTRACT: The binding pockets of extant enzymes feature precise positioning of amino acid residues that facilitate multiple complex transformations exploiting covalent and non-covalent interactions. Reversible covalent anchoring is extensively used as an efficient tool by Nature for activating modern enzymes such as esterases, dehydratases and also for proteins like opsins for the complex process of visual phototransduction. Here we construct paracrystalline amyloid surfaces through the self-propagation of short peptides which offer binding pockets exposed with arrays of imidazoles and lysines. As covalent catalysis is utilized by modern-day enzymes, these homogenous amyloid nanotubes exploit Schiff imine formation via the exposed lysines to efficiently hydrolyse both activated and inactivated esters. Controls where lysines were mutated with charged residues accessed similar morphologies but did not augment rate. The designed amyloid microphases thus foreshadow the generation of binding pockets of advanced proteins and have the potential to contribute to the development of functional materials.

Nature accesses vastly orthogonal chemical strategies to regulate complex multi-step chemical processes catalyzed by the highly evolved present day enzymes.[1] These extant biocatalysts, products of millions of years of evolution, feature well-defined three-dimensional architectures created from folding of long polymers of amino acids and offer specific binding pockets for small molecular guests.[1-3] Precise positioning of the amino acid residues in the active site is critical for catalysis through a sequence of cascade reactions.[1-4] Involvement of multiple active site residues is required for the complicated tasks of manipulation of protonation events, polarizing and activating the nucleophiles and electrophiles and so forth. Notably, in the regulation of complex biological processes, reversible covalent bond formation has also been extensively used as an efficient tool by Nature.[5-8] Direct covalent bonding for the enzyme or cofactor with the substrates has been seen including the formation of covalent intermediates such as acyl enzyme or Schiff base intermediate.[7] Enzymes such as serine protease, protein kinase and phosphatase utilize transient covalent bonds to improve substrate affinity and lower the activation energy.[5-8] Further, for the beautiful phenomenon of visual phototransduction, reversible Imine formation is exploited by opsin where the lysine side chain bonds reversibly with a chromophoric aldehyde.[7] Also, the biosynthetic shikimate pathway followed by dehydratases proceeds through imine formation between lysine side chain and the carbonyl group of the substrate. Mutating lysine results in sharp decline of activity, suggesting the importance of the reversible covalent bond.[8]

We asked whether a short amyloid-based peptide can use such covalent bonding between the catalyst and substrate to amplify the catalytic rates. Short peptides capable of accessing inherent

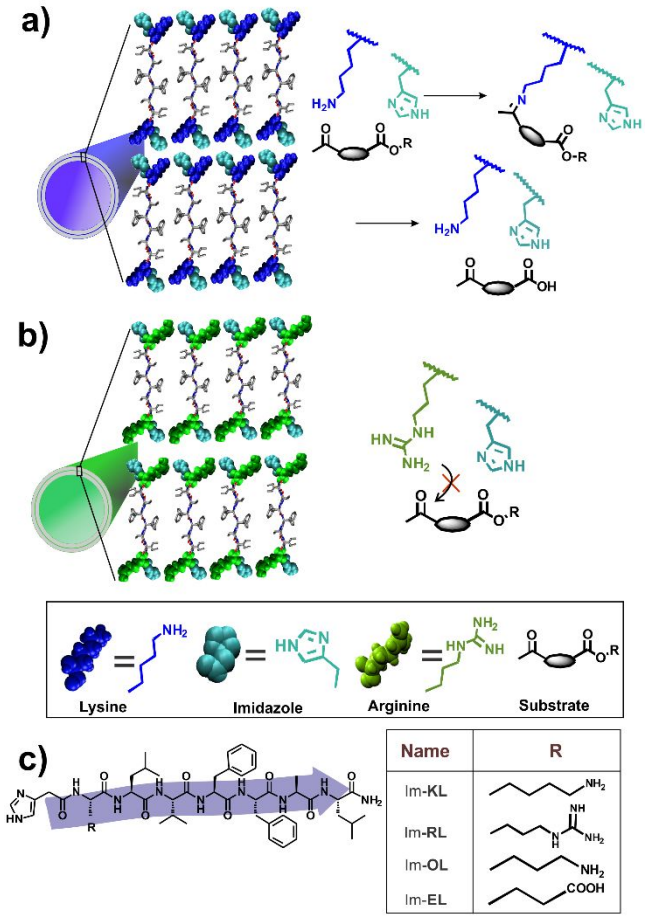

Figure 1. Schematic representation of the hydrolysis reaction facilitated through imine formation. a, b) Blue and green tube represents Im-**KL** and Im-**RL** nanotubes, c) structures of amyloid sequences.

repetitive structures of cross β amyloid folds have been argued as the primitive protein folds by works of Ulijn, Lynn, and Korendovych.[9-12] These offer solvent exposed binding surfaces to interact with diverse guests.[13] Herein, we report catalytic potential of one such amyloid phase, which exploits the process of covalent catalysis with exposed lysine side arms and imidazoles to show hydrolytic activity and cleave both activated and inactivated esters (Figure 1).

We used peptide fragment ^{17}LVFFA^{21} from the nucleating core of amyloid β 1-42, recognized as the fibrillar aggregates of

Alzheimer's disease.[14-15] This pentapeptide core has been known to access diverse morphologies.[14-15] The sequence H_2N-LVFFA-COOH was condensed with lysine and leucine residues at the N- and C-termini respectively. Further, the N terminal lysine residue was condensed with imidazole acetic acid leading to the sequence of Im-**K**LVFFA**L**-NH_2 (Im-**KL**, Figure 1). It was expected that the lysine coupled with imidazole group would be exposed to the solvent upon assembly enabling interaction with substrate. While the imidazole can assist in hydrolysis, the exposed lysine residues would be used for imine bond formation and thus can augment rates by covalent catalysis. This sequence assembled into homogenous nanotubular structures (diameter 50±10 nm) as observed under transmission electron microscopy (TEM, Figure 2a) and atomic force microscopy (AFM, Figure 2d, average height of nanotubes was 7.6 ±0.7 nm, Figure S1, SI). The β-sheet conformation of Im-**KL** assemblies was confirmed from circular dichroism (CD) and FTIR spectroscopy (Figure 2f, S2, SI). Powder X-ray diffraction (PXRD) had reflection at d-spacing of 4.65 Å and 10.62 Å corresponding to the distances of H-bonded β-strands and β-sheet laminates respectively (Figure 2f).[14b] To probe that indeed the charged lysines coupled with imidazoles are exposed to solvent, negatively charged Au-NP was added to the assemblies. Ordered arrays of nanoparticles were observed to be bound to the nanotubes (Figure S3, S4a). Control done with cationic AuNP did not result in specific binding (Figure S4b). To probe the binding capabilities of these nanotubes, we used a small hydrophobic fluorescent dye (coumarin 343). The β strands arranged in antiparallel fashion expose both the lysines and leucines side chains to solvent and thus can bind non-polar substrates.[12d,14b,15a] Confocal fluorescence microscopy revealed fluorescent structures when incubated with coumarin 343, thus supporting the binding capability of these assemblies (Figure 2e, Figure S5, SI for details and control).

We investigated the role of the lysine exposed Im-**KL** nanotubes to assist in the hydrolase like activity. Keto ester 4-nitrophenyl 4-oxopentanoate (**1**) featuring carbonyl group was synthesized with the expectation that it can form iminium intermediate upon binding to Im-**KL** (Figure 3a). As control, the lysine residue of the Im-**KL** group was mutated with arginine, generating the sequence Im-**RL** (Im-**R**LVFFA**L**). Im-**RL** would not be able to form such imine bonds due the presence of non-nucleophilic guanidine moiety in place of a primary amine (Figure 1). Im-**RL** assembled to form nanotubes with similar diameter of 46±4 nm, presumably due to the similar protonation states of lysine and arginine (Figure 2b). CD indicated similar β-sheet like conformation in assembled state of Im-**RL** (Figure S6s). Significantly, Im-**KL** showed an order of magnitude higher activity for **1** ($[v_i]_{Im\text{-}KL}$=5.6 ±0.5 μM min^{-1}, Figure 3c) compared to the control Im-**RL** ($[v_i]_{Im\text{-}RL}$=0.49±0.07 μM min^{-1}, ca. 11 fold at pH=8, Table S1, Figure 3b) suggesting the important role of lysine residues (no acylated Im-**KL** peptide was observed from HPLC).

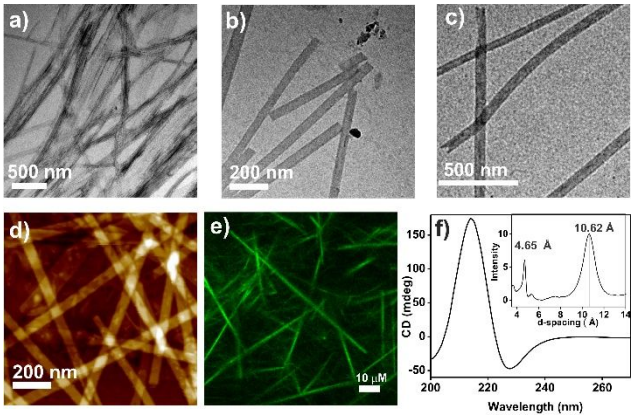

Figure 2. TEM micrographs of a) Im-**KL** b) Im-**RL**, c) Im-**OL**, AFM of d) Im-**KL**, e) Confocal microscopy image of coumarin-343 (λ_{ex} = 488 nm) bound Im-**KL**, f) CD spectra and PXRD (inset) of Im-**KL**.

An analogous substrate lacking the keto group (**2**) was synthesized (Figure 3a). Notably, Im-**KL** showed only a modest enhancement in activity with **2** when compared to Im-**RL** ($[v_i]_{Im\text{-}KL}$=6.2±0.1 μM min^{-1}, $[v_i]_{Im\text{-}RL}$= 3.1±0.5 μM min^{-1}) which supports the activating role of the lysines for the keto containing substrates (Figure 3b). The hydrolysis reactions followed typical Michaelis-Menten kinetics (Figure S7, Table S2). The substrate affinity of the lysine nanotubes towards the keto containing substrate was much higher compared to the control arginine exposed nanotubes as reflected from the K_m value of **1** for Im-**KL** which was 3 fold lower compared to Im-**RL**. The catalytic efficiency of Im-**KL** for the keto containing substrate was also following a similar trend (Table S2). Reduction in presence of excess $NaBH_3CN$ was done to trap the kinetically unstable imine of **1** with Im-**KL** to the corresponding amine which was confirmed by Mass spectrometry (SI). To further investigate the role of side chain of the amino acid at 16th position, we mutated the cationic lysine with negatively charged glutamic acid (Im-**EL**, Figure 1). Im-**EL** did not assemble to form homogenous nanotube but instead accessed sheet like morphologies (Figure S8). Activity was found to be significantly lower due to lack of the primary amine for the imine bond and also due to possible increment of pKa of neighboring imidazoles (Figure 3c).

To check the role of side chain length of the amine and also to investigate the effect of neighboring strands of the cross β assembly, lysine (four methylenes) was mutated with its shorter congener ornithine (3 methylenes) to generate Im-**OL** (Im-**O**LVFFA**L**). Im-**OL** assembled to form morphologically similar nanotubes of diameter 40±5 nm (Figure 2c). Higher activity was observed for Im-**OL** compared to Im-**RL** ($[v_i]$=3.6±0.6 μM min^{-1}, Figure 3c) further supporting the importance of amines.

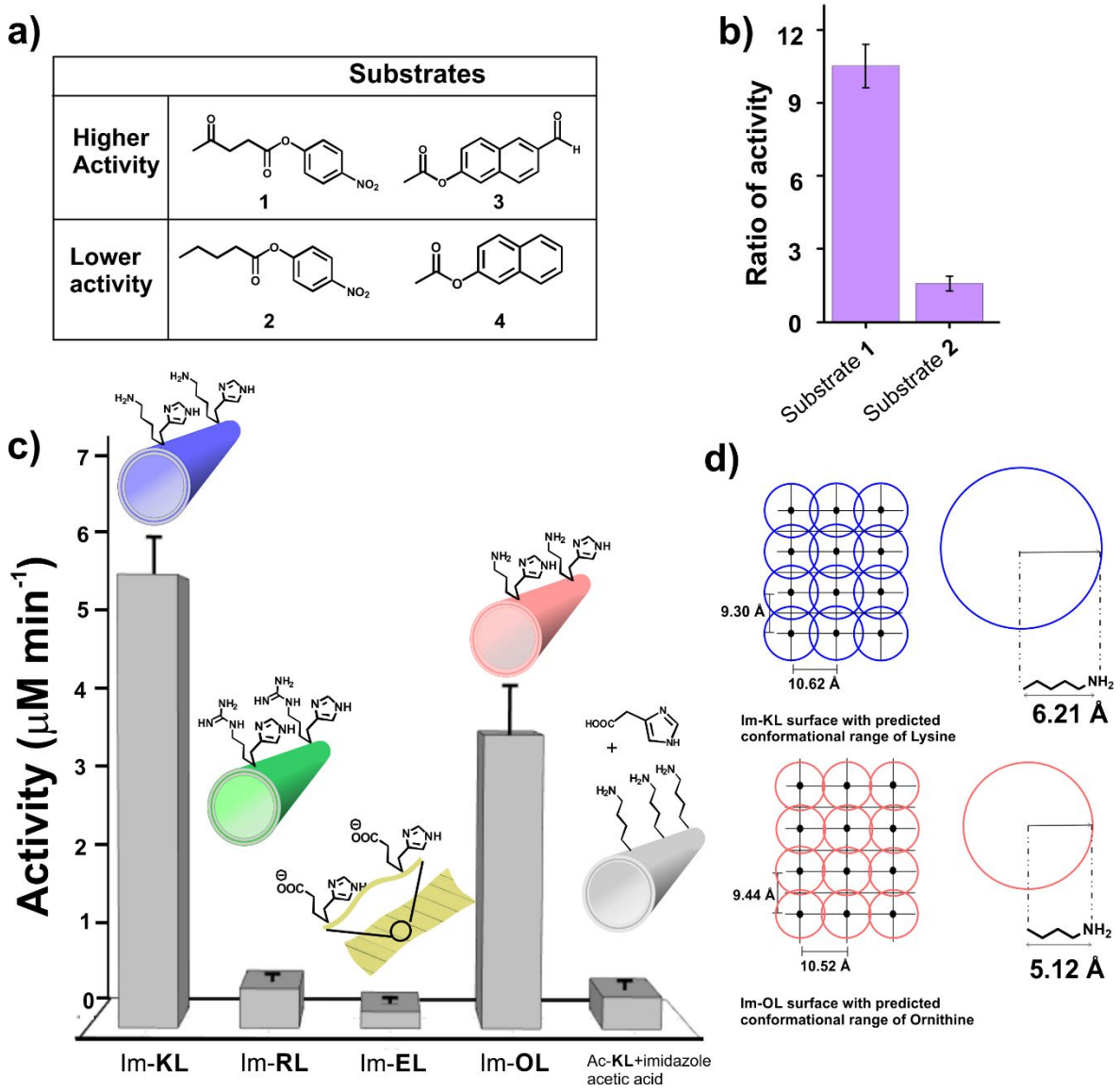

Figure 3. a) Chemical structure of substrates b) Bar diagram of the ratio of hydrolysis rates by Im-**KL** and Im-**RL** for **1** and **2**. c) Bar diagram of hydrolysis rate of **1** by Im-**KL**, Im-**RL**, Im-**EL**, Im-**OL** and Ac-**KL** in presence of imidazoleacetic acid, [Peptide]= 1mM, [Substrate]= 50 μM.d) Grids showing the amine accessible surface of Im-**KL** and Im-**OL** nanotubes with the average conformational ranges indicated by blue and red circles respectively.

However, the activity for Im-**OL** was lower than Im-**KL**, indicating the assistance from the exposed amines from the proximal strands of the cross β structures. PXRD patterns suggested larger accessible surface for the lysines versus the ornithines (Figure 3d and Figure S9, see SI for details). Further, Im-**KL** nanotubes were disassembled with hexafluoroisopropanol (HFIP, SI). Disassembly of secondary structure was suggested from loss of CD signals (Figure S10a, SI) and absence of any distinct morphologies in TEM (Figure S10b, SI). The disassembled Im-**KL** aged for ca. 1 h showed substantially lower activity compared to the nanotubes (Table S1). Significantly, disassembled Im-**RL** showed similar activity to that found for disassembled Im-**KL**, thus suggesting the role of the neighboring amines generated from assembled structures for covalent catalysis (Figure 3d, Table S1). We detached the residues responsible for the activity of Im-**KL** and added imidazole acetic acid separately to Ac-**KL** (Ac-**K**LVFFA**L**, assembles to form homogenous nanotubes[11-12] and did not have measurable intrinsic hydrolase activity). Compared to Im-**KL**, the activity dropped to 14-fold, indicating the importance of a surface with arrays of imidazoles and lysines ($[v_i]$=0.40±0.09 μM min^{-1}, Figure 3c, Table S1, imidazole acetic acid was expected to be near to the positively charged nanotubes).

For spectroscopic investigation of the imine formation, fluorescent aldehyde 6-hydroxy 2-naphthaldehyde (**Ar-CHO**) was used. Naphthaldehyde backbone is known for its binding to amyloid phases as it features in molecular histological stains like Congo Red.[15b] **Ar-CHO** registered quenching upon addition to Im-**KL**, suggesting the formation of Schiff base as the lone pair of imine nitrogen is known to quench through nonradiative channel (Figure S11, SI).[17] However, when **Ar-CHO** was incubated with the control nanotubes of Im-**RL**, the fluorescence intensity registered an enhancement as expected from the binding of the dye to the

hydrophobic environment of the nanotubular surfaces (Figure S11, SI). Further, hydrophobic fluorophores such as ANS and pyrene which lack the carboxyl group, showed enhancement of intensities upon binding to the Im-**RL** and Im-**KL** nanotubes (Figure S12, SI).[18]

We expected that this assistance of a covalent linkage can broaden the scope of the substrates that are kinetically more stable. Hence, we investigated the ability of the Im-**KL** nanotubes to hydrolyse less activated esters. We acetylated the phenolic group of **Ar-CHO** to form **3** (Figure 3a). Interestingly, Im-**KL** showed facile hydrolysis of **3** as monitored by UV-Visible spectroscopy (6.6±0.8 μM min^{-1}, followed at 310 nm, Figure S13, S14, SI). This rate was 7.9 fold higher compared to Im-**RL** nanotubes (0.83±0.08 μM min^{-1}) thus underpinning the importance of covalent linkage for the development of an efficient catalytic system (Figure 4a). The hydrolytic activity for Im-**KL** could also be reflected from the time course generation of fluorescent entangled networks in epifluorescence microscopy, signifying the formation of surface-bound fluorescent **Ar-CHO** (Figure 4b). As a control, **4** was synthesized which will form 2-naphthol after hydrolysis (Figure 3a). Due to the symmetrically forbidden n→π* transitions (low ε of 527 $M^{-1}cm^{-1}$), fluorescence spectroscopy was used to monitor the product formation.[19] The rates for **4** for Im-**KL** was similar to that shown by Im-**RL** which further underpinned the importance of the covalent anchoring of the substrates ($[v_i]_{Im\text{-}KL}$=0.79±0.09 μM min^{-1}, $[v_i]_{Im\text{-}RL}$=0.52±0.09 μM min^{-1}, Figure 4a, Figure S15). From HPLC with Im-**KL**, the conversions were found to be 21 % after 30 min for **3**, whereas for **4**, it was only 2%, thus further stressing the effectiveness of the reported system (Figure S16-S17). In order to compare the activity of Im-**KL** with native enzyme carbonic anhydrase (CA), a standard substrate 4-nitrophenyl acetate was used. Although the catalytic efficiency was around 2 orders of magnitude lower (2.4±0.3 $M^{-1}sec^{-1}$) than CA, on the basis of molecular mass, the activity was only 22.7-fold lower than the evolved enzyme.[20]

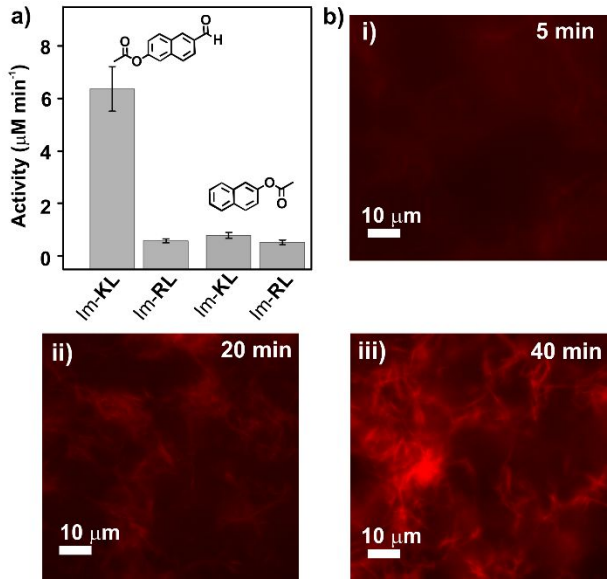

Figure 4. a) Bar diagram of initial rates with Im-**KL** and Im-**RL**. [peptide]=1mM, [substrate]=50 μM. b) Representative images of time resolved epifluorescence microscopy of Im-**KL** in presence of **3**.

In summary, this work builds on the capabilities of short amyloid peptide assemblies to not only act as efficient hydrolases but also demonstrate advanced traits such as covalent catalysis. The microenvironment featuring lysines and imidazoles shows higher substrate affinity and accelerates catalytic activity. Importantly, these peptide nanotubes promoted the hydrolysis of inactivated esters, thus opening up the possibility of designing new materials capable of performing catalysis on expanded substrate scope. The simplicity of the peptide sequences which offers multiple amino acid residues on the paracrystalline phases foreshadows the prebiotic origins of binding pockets of advanced proteins. This observation also supports the covalent hypothesis of involving covalent bond formation in intermediate as exploited by Nature for evolved enzymes.

ASSOCIATED CONTENT

Supporting Information

The Supporting Information is available free of charge on the ACS Publications website. Experimental procedures, details of kinetic analysis, synthesis and characterization of molecules.

AUTHOR INFORMATION

Corresponding Author

*dasd@iiserkol.ac.in
ORCID Dibyendu Das:0000-0001-6597-8454

Notes

The authors declare no competing financial interests.

ACKNOWLEDGMENT

D.D. is thankful to Nano Mission Grant (SR/NM/NS-1082/2015), DST, GOI for financial assistance. BS and AC acknowledge CSIR, India. We thank Syed Pavel Afrose for his valuable help.

REFERENCES

1. a) Woese, C. R. On the Evolution of Cells. *Proc. Natl. Acad. Sci. USA* **2002**, *99*, 8742–8747; b) Li, L.; Francklyn, C.; Carter, C. W. Aminoacylating Urzymes Challenge the RNA World Hypothesis. *J. Biol. Chem*. **2013**, *288*, 26856−26863.
2. Baldwin, A. J.; Knowles, T. P. J.; Tartaglia, G. G.; Fitzpatrick, A. W.; Devlin, G. L.; Shammas, S. L.; Waudby, C. A.; Mossuto, M. F.; Meehan, S.; Gras, S. L.; Christodoulou, J.; Anthony-Cahill, S. J.; Barker, P. D.; Vendruscolo, M.; Dobson, C. M. Metastability of Native Proteins and the Phenomenon of Amyloid Formation. *J. Am. Chem. Soc.* **2011**, *133*, 14160-14163.
3. a) Zhang, Y.; Tsitkov, S.; Hess, H. Complex Dynamics in a Two-Enzyme Reaction Network with Substrate Competition. *Nat. Catal*. **2018**, *1*, 276-281; b) Zhao, X.; Palacci, H.; Yadav, V.; Spiering, M. M.; Gilson, M. K.; Butler, P.J.; Hess, H.; Benkovic, S. J.; Sen, A. Substrate-Driven Chemotactic Assembly in an Enzyme Cascade. *Nat. Chem.* **2018**, *10*, 311-317;
4. a) Somasundar, A.; Ghosh, S.; Mohajerani, F.; Massenburg, L. N.; Yang, T.; Cremer, P. S.; Cremer, D.; Sen, A. Positive and Negative Chemotaxis of Enzyme-Coated Liposome. *Nat. Nanotechnol.* **2019**, *14*, 1129-1134; b) Burton, A. J.; Thomson, A. R.; Dawson, W. M.; Brady, R. L.; Woolfson, D. N. Installing Hydrolytic Activity into a Completely de Novo Protein Framework. *Nat. Chem*. **2016**, *8*, 837−844; c) Kaplan, J.; DeGrado, W. F. De novo Design of Catalytic Proteins. *Proc. Natl. Acad. Sci. USA* **2004**, *101*, 11566-11570.
5. a) Huang, Y.; Bolen, D. W. Covalent Bond Changes as a Driving Force in Enzyme Catalysis. *Biochemistry* **1993**, *32*, 9329–9339; b) Zhang, X. Y.; Houk, K. N. Why Enzymes Are Proficient Catalysts: Beyond the Pauling Paradigm. *Acc. Chem. Res*. **2005**, *38*, 379-385.
6. a) Wang, Z.; Cole, P. A. Catalytic Mechanisms and Regulation of Protein Kinases. *Methods Enzymol*. **2014**, *548*, 1-21; b) MacDonald, M. J.; Lavis, L. D.; Hilvert, D.; Gellman, S. H. Evaluation of the Ser-His Dipeptide, a Putative Catalyst of Amide and Ester Hydrolysis. *Org. Lett.* **2016**, *18*, 3518–3521

7. a) Shichida, Y.; Matsuyama, T. Philos. Evolution of Opsins and Phototransduction. *Trans. R. Soc. B*. **2009**, *364*, 2881-2895; b) Neri, S.; Garcia Martin, S.; Pezzato, C.; Prins, L. J. Photoswitchable Catalysis by a Nanozyme Mediated by a Light-Sensitive Cofactor. *J. Am. Chem. Soc.* **2017**, *139*, 1794–1797.
8. Leech, A. P.; James, R.; Coggins, J. R.; Kleanthous. C. Mutagenesis of Active Site Residues in type I Dehydroquinase from Escherichia Coli. Stalled Catalysis in a Histidine to Alanine Mutant. *J. Biol. Chem.* **1995**, *270*, 25827–25836.
9. a) Greenwald, J.; Riek, R. On the Possible Amyloid Origin of Protein Folds. *J. Mol. Biol.* **2012**, *421*, 417-426; b) Greenwald, J.; Friedmann, M. P.; Riek, R. Amyloid Aggregates Arise from Amino Acid Condensations under Prebiotic Conditions. *Angew. Chem. Int. Ed.* **2016**, *55*, 11609−11613; c) Carny, O.; Gazit, E. A Model for the Role of Short Self-Assembled Peptides in the Very Early Stages of the Origin of Life. *FASEB J*. **2005**, *19*, 1051-1055; d) Ashkenasy, G.; Hermans, T. M.; Otto, S.; Taylor, A. F. Systems Chemistry. *Chem. Soc. Rev.* **2017**, *46*, 2543-2554.
10. Friedmann, M. P.; Torbeev, V.; Zelenay, V.; Sobol, A.; Greenwald, J.; Riek, R. Towards Prebiotic Catalytic Amyloids Using High Throughput Screening. *PLoS One* **2015**, *10*, e0143948;
11. a) Rufo, C. M.; Moroz, Y. S.; Moroz, O. V.; Stöhr, J.; Smith, T. A.; Hu, X.; DeGrado, W. F.; Korendovych, I. V. Short Peptides Self-Assemble to Produce Catalytic Amyloids. *Nat. Chem*. **2014**, *6*, 303-309; b) Rubinov, B.; Wagner, N.; Rapaport, H.; Ashkenasy, G. Self –Replicating Amphiphilic Beta- Sheet Peptides. *Angew. Chem., Int. Ed.* **2009**, *48*, 6683−6686; c) Zhang, C.; Xue, X.; Luo, Q.; Li, Y.; Yang, K.; Zhuang, X.; Jiang, Y.; Zhang, J.; Liu, J.; Zou, G.; Liang, X. J. Self-Assembled Peptide Nanofibers Designed as Biological Enzymes for Catalyzing Ester Hydrolysis. *ACS Nano* **2014**, *8*, 11715−23; d) Guler, M. O.; Stupp, S. I. A Self-Assembled Nanofiber Catalyst for Ester Hydrolysis. *J. Am. Chem. Soc.* **2007,** *129,* 12082-12083; e) Zhang, C.; Shafi, R.; Lampel, A.; MacPherson, D.; Pappas, C.; Narang, V.; Wang, T.; Madarelli, C.; Ulijn, R. V. Switchable Hydrolase Based on Reversible Formation of Supramolecular Catalytic Site Using a Self-Assembling Peptide. *Angew. Chem. Int. Ed*. **2017**, *56*, 14511- 14515; f) Gao, Y.; Zhao, F.; Wang, Q.; Zhang, Y.; Xu, B. Small Peptide Nanofibers as the Matrices of Molecular Hydrogels for Mimicking Enzymes and Enhancing the Activity of Enzymes. *Chem. Soc. Rev*. **2010**, *39*, 3425– 3433; g) Frederix, P. W. J. M.; Scott, G. G.; Abul-Haija, Y. M.; Kalafatovic, D.; Pappas, C. G.; Javid, N.; Hunt, N. T.; Ulijn, R. V.; Tuttle, T. Exploring the Sequence Space for (Tri-)Peptide Self-Assembly to Design and Discover New Hydrogels. *Nat. Chem*. **2015**, *7*, 30-37; h) Reja, A.; Afrose, S. P.; Das, D. Aldolase Cascade Facilitated by Self-Assembled Nanotubes from Short Peptide Amphiphiles. *Angew. Chem. Int. Ed*. **2020**, https://doi.org/10.1002/ange.201914633; i) Al-Garawi, Z. S.; McIntosh, B. A.; Neill-Hall, D.; Hatimy, A. A.; Sweet, S. M.; Bagley, M. C.; Serpell, L. C. The amyloid architecture provides a scaffold for enzyme-like catalysts. *Nanoscale* **2017**, *9*, 10773–10783
12. a) Tena-Solsona, M.; Nanda, J.; Diaz-Oltra, S.; Chotera, A.; Ashkenasy, G.; Escuder, B. Emergent Catalytic Behaviour of Self-Assembled Low Molecular Weight Peptide-Based Aggregates and Hydrogels. *Chem. Eur. J.* **2016**, *22*, 6687−6694; b) Singh, N.; Kumar, M.; Miravet, J. F.; Ulijn, R. V.; Escuder, B. Peptide-Based Molecular Hydrogels as Supramolecular Protein Mimics. *Chem. Eur. J*. **2017**, *23*, 981−993; c) Schneider, J. P.; Pochan, D. J.; Ozbas, B.; Rajagopal, K.; Pakstis, L.; Kretsinger, J. Responsive Hydrogels from the Intramolecular Folding and Self-Assembly of a designed Peptide. *J. Am. Chem. Soc.* **2002**, *124*, 15030-15037; d) Omosun, T. O.; Hsieh, M. C.; Childers, W. S.; Das, D.; Mehta, A. K.; Anthony, N. R.; Pan, T.; Grover, M. A.; Berland, K. M.; Lynn, D. G. Catalytic Diversity in Self-Propagating Peptide Assemblies. *Nat. Chem*. **2017**, *9*, 805-809; e) Mehta, A.K.; Lu, K. ; Childers, W. S.; Liang, Y.; Dublin, S. N.; Dong, J. ; Snyder, J. P. ; Pingali, S. V.; Thiyagarajan, P.; Lynn, D. G. Facial Symmetry in Protein Self-Assembly. *J. Am. Chem. Soc.* **2008**, *130*, 9829–9835; f) Kroiss, D.; Ashkenasy, G.; Braunschweig, A. B.; Tuttle, T.; Ulijn, R. V. Catalyst: Can Systems Chemistry Unravel the Mysteries of the Chemical Origins of Life? *Chem*, **2019**, *5*, 1917-1923.
13. a) Wei, G.; Su, Z.; Reynolds, N. P.; Arosio, P.; Hamley, I. W.; Gazit, E.; Mezzenga, R. Self-Assembling Peptide and Protein Amyloids: from Structure to Tailored Function in Nanotechnology. *Chem. Soc. Rev*. **2017**, *46*, 4661-4708; b) Branco, M. C.; Sigano, D. M.; Schneider, J. P. Materials from Peptide Assembly: towards the Treatment of Cancer and Transmittable disease. *Curr. Opin. Chem. Biol*. **2011**, *15*, 427–434;
c) Kapil, N.; Singh, A.; Singh, M.; Das, D. Efficient MoS2 Exfoliation by Cross-β-Amyloid Nanotubes for Multistimuli-Responsive and Biodegradable Aqueous Dispersions. *Angew. Chem. Int. Ed.* **2016**, *55,* 7772-7776; d) Makam, P.; Yamijala, S.; Tao, K. ; Shimon, L.; Eisenberg, D.; Sawaya, M.; Wong, B.; Gazit, E. Nonproteinaceous Hydrolase Comprised of a Phenylalanine Metallo-Supramolecular Amyloid-like Structure. *Nat. Catal.* **2019**, *2*, 977–985; e) Singh, A.; Kapil, N.; Yenuganti, M.; Das, D. Exfoliated Sheets of MoS2 Trigger Formation of Aqueous Gels with Acute NIR Light Responsiveness. *Chem. Commun*. **2016**, *52*, 14043-14046 f) Knowles, T. P. J.; Mezzenga, R. Amyloid Fibrils as Building Blocks for Natural and Artificial Functional Materials. *Adv. Matter*. **2016**, *28*, 6546-6561.
14. a) Elkins, M. R.; Wang, T.; Nick, M.; Jo, H.; Lemmin, T.; Prusiner, S. B.; DeGrado, W. F.; Stoehr, J.; Hong, M. Structural Polymorphism of Alzheimer's β-Amyloid Fibrils as Controlled by an E22 Switch: A Solid-State NMR Study. *J. Am. Chem Soc*. **2016**, *138*, 9840-9852; b) Li, S.; Sidorov, A. N.; Mehta, A. K.; Bisignano, A. J.; Das, D.; Childers, W. S.; Schuler, E.; Jiang, Z.; Orlando, T. M.; Berland, K.; Lynn, D. G. Neurofibrillar Tangle Surrogates: Histone H1 Binding to Patterned Phosphotyrosine Peptide Naonotubes. *Biochemistry* **2014**, *53*, 4225-4227.
15. a) Kapil, N.; Singh, A.; Das, D. Cross-β Amyloid Nanohybrids Loaded With Cytochrome C Exhibit Superactivity in Organic Solvents. *Angew. Chem. Int. Ed*. **2015**, *54*, 6492-6495; b) Childers, W. S.; Mehta, A. K.; Lu, K.; Lynn, D. G. Templating Molecular Arrays in Amyloid's Cross-β Grooves. *J. Am. Chem. Soc*. **2009**, *131*, 10165-10172;
16. a) Goodwin, J.T.; Lynn, D.G. Template Directed Synthesis: Use of a Reversible Reaction. *J. Am. Chem. Soc.* **1992**, *114*, 9197-9198; b) Corbett, P. T.; Leclaire, J.; Vial, L.; West, K. R.; Wietor, J. L.; Sanders, J. K. M.; Otto, S. Dynamic Combinatorial Chemistry. *Chem. Rev.* **2006**, *106*, 3652– 3711.
17. a) Lassila, J. K.; Baker, D; Herschlag. D. Origins of Catalysis by Computationally Designed Retroaldolase Enzymes. *Proc. Natl. Acad. Sci. USA* **2010**, *107*, 4937–4942; b) Obexer, R.; Godina, A.; Garrabou, X.; Mittl, P. R. E.; Baker, D.; Griffiths, A. D.; Hilvert, D. Emergence of a catalytic tetrad during evolution of a highly active artificial aldolase. *Nat. Chem.* **2016**, *9*, 50– 56; c) Jiang, L.; Althoff, E. A.; Clemente, F. R.; Doyle, L.; Röthlisberger, D.; Zanghellini, A.; Gallaher, J. L.; Betker, J. L.; Tanaka, F.; Barbas, C. F.; Hilvert, D.; Houk, K. N.; Stoddard, B. L.; Baker, D. De Novo Computational Design of Retro-Aldol Enzymes. *Science* **2008**, *319*, 1387-1391.
18. Cardamone, M. N.; Puri, K. Spectrofluorimetric Assessment of the Surface Hydrophobicity of Proteins. *Biochem J.* **1992**, *282*, 589–593
19. Nagakura, S. ; Gouterman, M. Effect of Hydrogen Bonding on the Near Ultraviolet Absorption of Naphthol *J. Chem. Phys.* **1957**, *26*, 881–886.
20. Verpoorte, J. A.; Mehta, S.; Edsall, J. T. Esterase activities of human carbonic anhydrases B and C. *J. Biol. Chem.* **1967**, *242*, 4221–4229.

Table of Contents

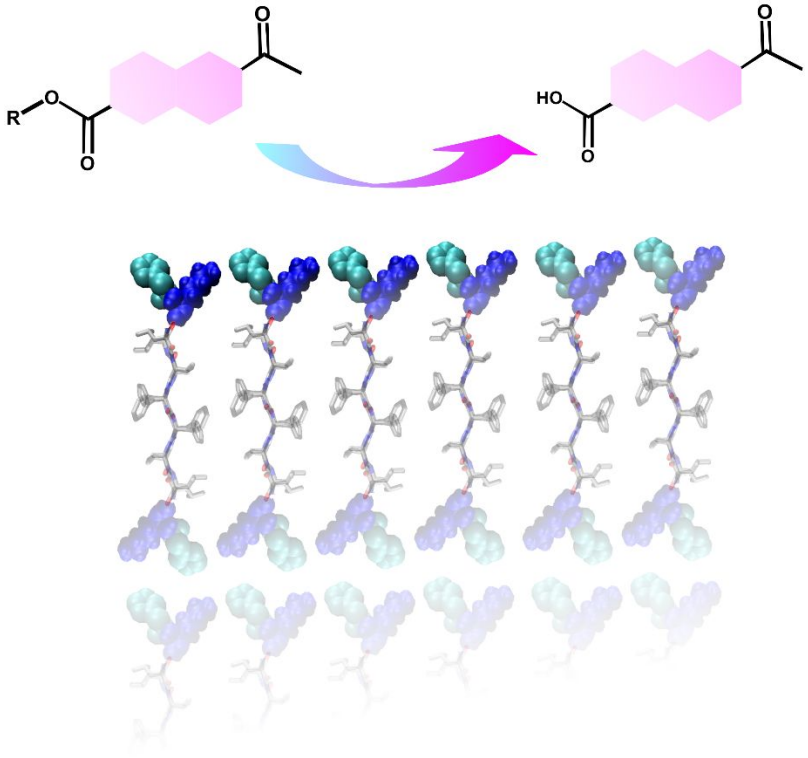
O
R
O
O
HO
O
O

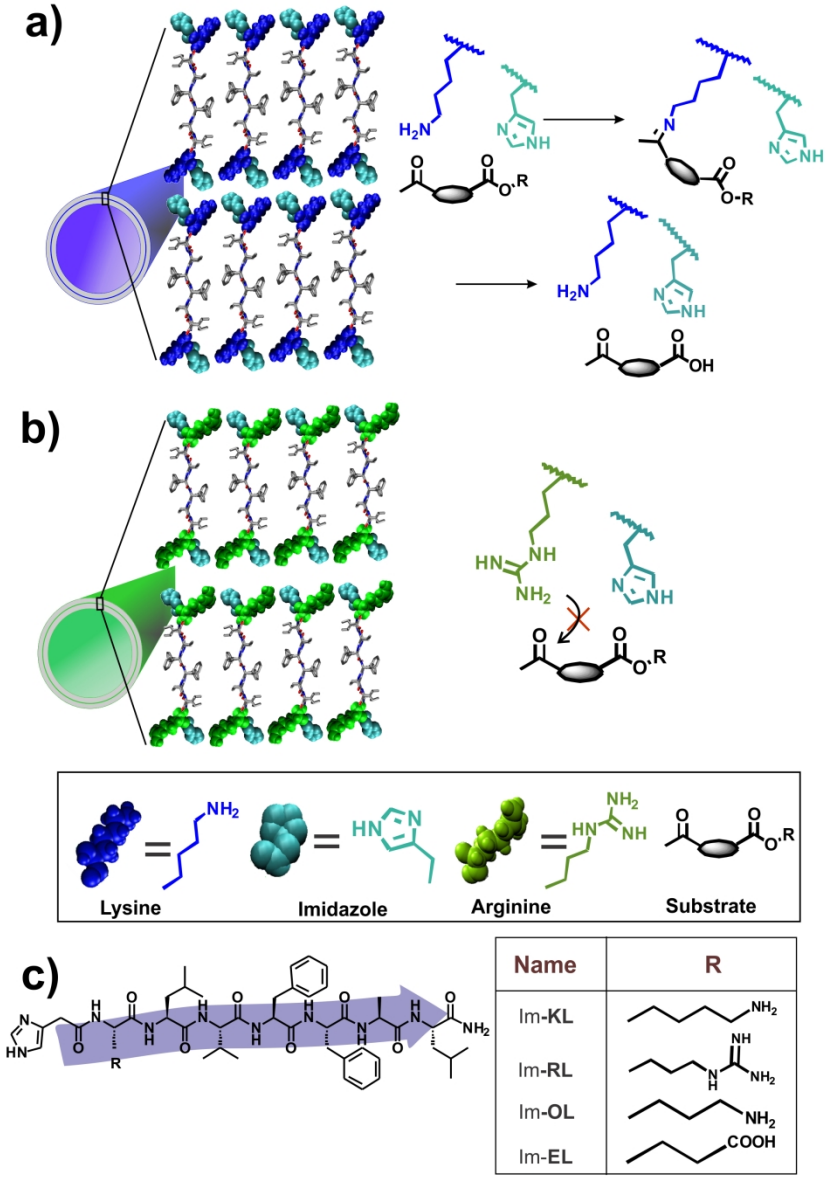
a)
b)
Lysine
Imidazole
Arginine
Substrate
c)
Name
R
Im-KL
Im-RL
Im-OL
Im-EL

Figure 1

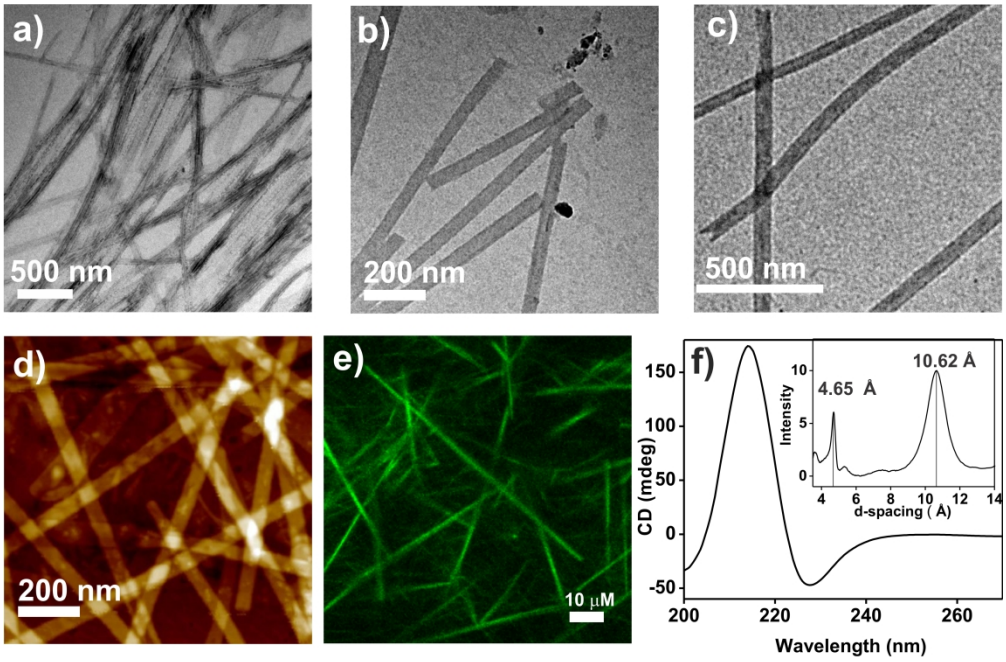
a)
500 nm
b)
200 nm
c)
500 nm
d)
200 nm
e)
10 μM
f)
CD (mdeg)
150
100
50
0
-50
200
220
240
260
Wavelength (nm)
Intensity
10
5
0
4.65 Å
10.62 Å
4
6
8
10
12
14
d-spacing (Å)

Figure 2

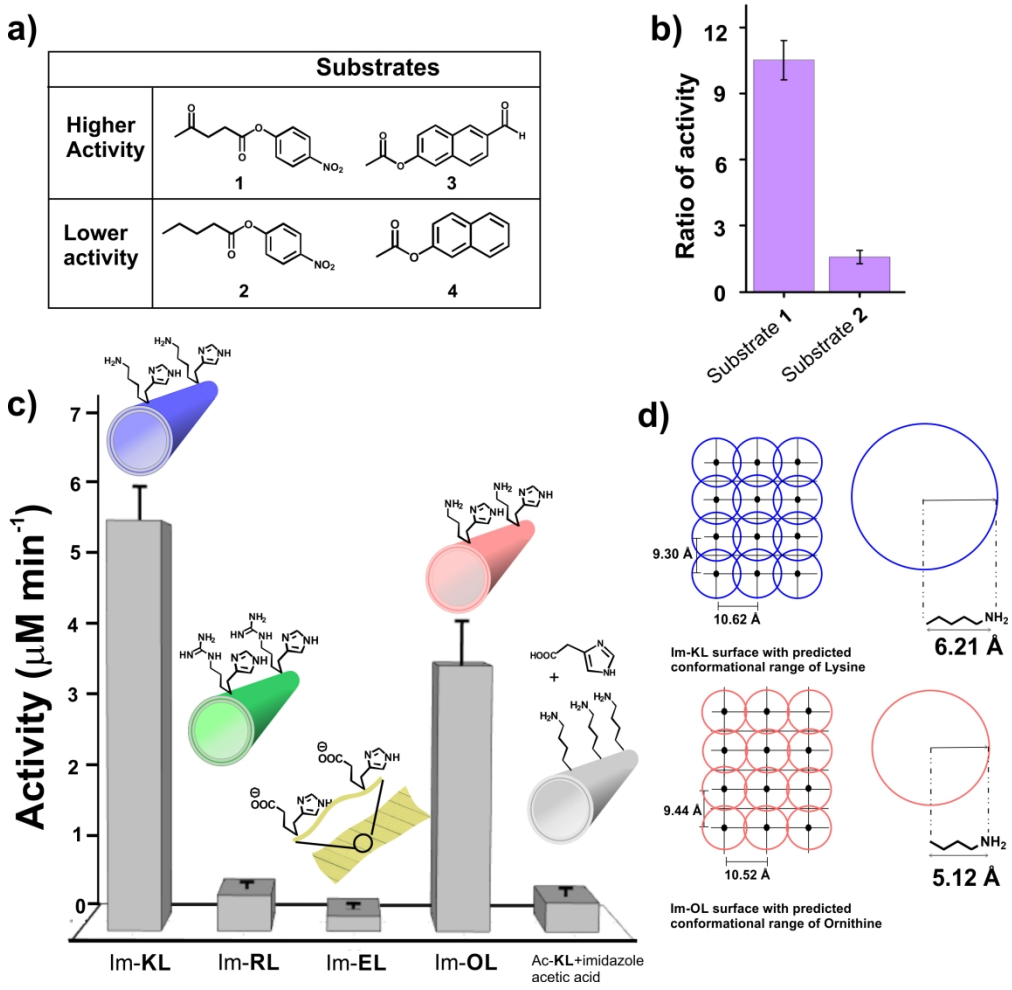
a)
Substrates
Higher Activity
Lower activity
1
2
3
4
b)
Ratio of activity
12
9
6
3
0
Substrate 1
Substrate 2
c)
Activity (μM min-1)
7
6
5
4
3
2
1
0
Im-KL
Im-RL
Im-EL
Im-OL
Ac-KL+imidazole acetic acid
d)
9.30 Å
10.62 Å
6.21 Å
Im-KL surface with predicted conformational range of Lysine
9.44 Å
10.52 Å
5.12 Å
Im-OL surface with predicted conformational range of Ornithine

Figure 3

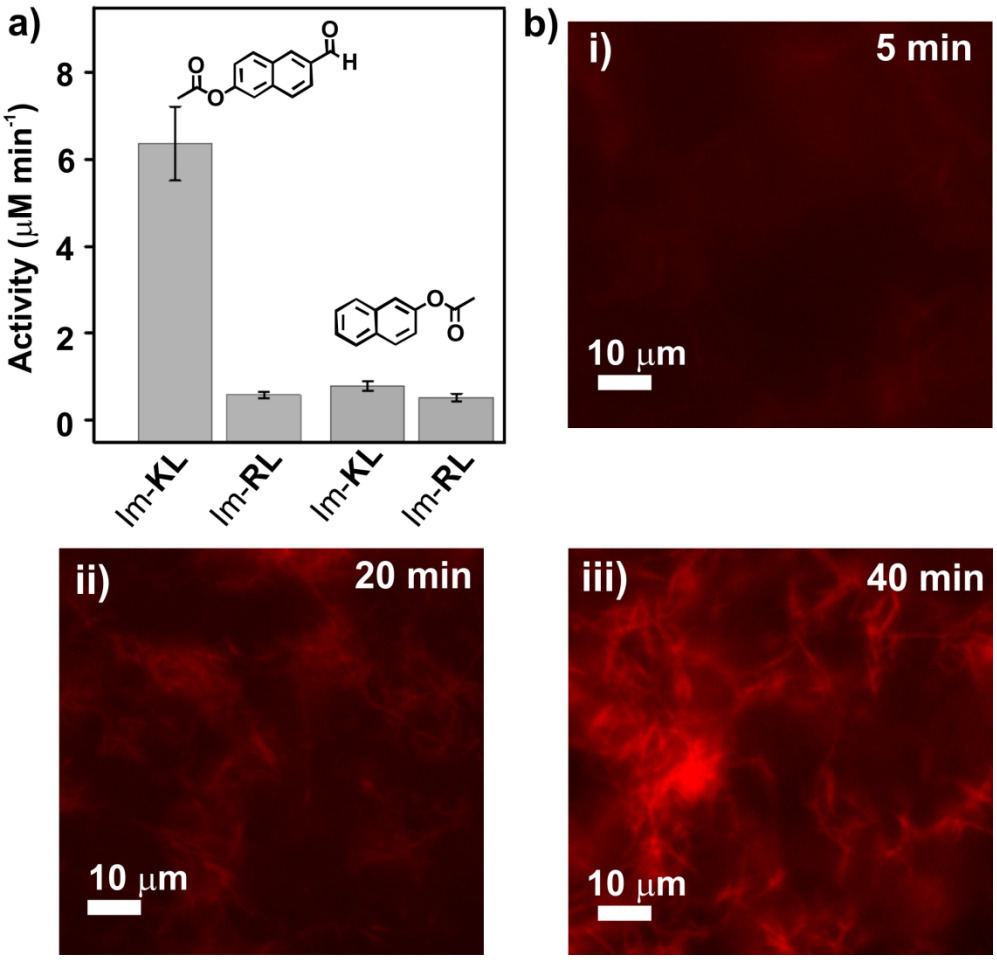
a)
b)
Activity (μM min-1)
0
2
4
6
8
Im-KL
Im-RL
Im-KL
Im-RL
i)
5 min
10 μm
ii)
20 min
10 μm
iii)
40 min
10 μm

Figure 4